International Research Journal of Engineering and Technology (IRJET) e-ISSN: 2395-0056
Volume: 10 Issue: 08 | Aug 2023 www.irjet.net p-ISSN: 2395-0072

Sol-gel auto-combustion produced gamma irradiated $Ni_{1-x}Cd_xFe_2O_4$ nanoparticles:TGA, UV-Vis spectra, and Raman spectroscopy

Manisha R. Patil[a], S.D. More[b], K.K. Kadam[b] , K.M. Jadhav [b]

[a]*Department of Physics, Deogiri College, Aurangabad 431001 INDIA*
[b]*Department of Physics, Dr. Babasaheb Ambdekar Marathwada University Aurangabad431001 INDIA*

Abstract

This work discusses the thermo gravimetric analysis (TGA), UV-Vis spectroscopic absorption, and Raman active modes of gamma-irradiated $Ni_{1-x}Cd_xFe_2O_4$NPs with a total dose of 50 Mrad. $Ni_{1-x}Cd_xFe_2O_4$NPs were made using the wet-chemical sol-gel assisted auto-combustion method (x = 0.0 and 0.1). $Ni_{1-x}Cd_xFe_2O_4$NPs' thermal study and physical characteristics revealed that they were exothermic between 150 and 600 °C and endothermic at that temperature. To support the phase formation study, the specific active modes T2g (1), T2g (2), T2g (3), and A1g in the Raman spectra were examined.$Ni_{1-x}Cd_xFe_2O_4$NPs (x = 0.0 and 0.1) were reported to have UV-Vis spectral absorption values of at λ = ~292.4 Å; ~340.2 Å; and 340.2 for $NiFe_2O_4$ NPs and ~340.77 Å; ~563.28 Å for $Ni_{1-x}Cd_xFe_2O_4$NPs exposed to gamma radiation. Using a Tauc's plot and the "Kubelka-Munk function," which was claimed to be between 1.41 and 1.5 eV, the optical bandgap was calculated.

Keywords: *TGA; Ferrite; NPs; Raman spectra; UV-Vis spectra, gamma irradiation*

1. Introduction

Ever since humans first began to evolve, "iron" and its oxides have been associated with human culture[1, 2]. Since antiquity, ferrites have been recognized as the stones that may attract and magnetize when exposed to an external magnetic field[3]. The researchers have been examining the cubic spinel ferrite's structural, morphological, electrical, and magnetic properties as well as all of its potential uses. The crucial subgroup of magnetic materials is made up of mixed transition metal oxides, which are frequently used for catalytic activities such as selective oxidation, selective reduction, dehydrogenation, semi conductive characteristics etc.[4].Studies has focused on nano crystalline materials because they offer a fresh and superior physical and chemical prospective that is not yet expressed with the bulk. These materials range in size from 1 nm to 100 nm. Spinel, which represent ferrites' significance in all potential sectors, have been grouped into three major classes based on their crystal structure, like $ZnFe_2O_4$, $NiFe_2O_4$, $Zn/NiFe_2O_4$, $CoFe_2O_4$, $MnFe_2O_4$, and $MgFe_2O_4$, etc.[5].The general specification of the ferrites' structural architecture is as follows[6, 7];

$$[M_{1-i}Fe_i]^A\left[M_iFe_{(2-i)}\right]^B O_4 \qquad (1)$$

It's interesting to note that ferrite still has the best magnetic and electrical characteristics, which makes them adaptable materials with high resistivity, minimal dielectric losses, mechanical hardness, and high Currie temperature. These ferrites are suited for high-frequency applications because to their chemical stability. The spinels also possess stunning physical and chemical characteristics, including better permeability, fewer eddy current losses, and higher saturation magnetization[8, 9]etc. Owing to their prospective uses in storage devices and high-frequency device applications, interest in nano crystalline ferrite has continued to grow[10, 11]. multiple imaging methods, pharmaceutical, the spatial and temporal resolution of diagnostic techniques [12], antibacterial, surgical implants, genetic engineering [13], medical appliances, particularly in the sterilization process [14], thus they have a significant potential for applications in the field of biomedicine [15, 16].The surface's magneto crystalline anisotropy, spins' canting, a super paramagnetic motion, and shape recovery[17].Nickel ferrite are suitable for catalytic activities, transformer core [18, 19], etc. inductors, electric motors, and many more.Among the range of spinel-type ferrites, nickel ferrite $(Ni_{1-x}Fe_x)[Ni_xFe_{2-x}]\ O_4$ has been focused on due to various applications. $NiFe_2O_4$ belongs to an inverse type spinel structure with Ni^{2+} on O_h [B]-site; and Fe^{3+} distributed equally at O_h [B]-site and T_d [A]-site. It was aimed to expand the unit cell of $NiFe_2O_4$; or increasing lattice constant by doping of the divalent cadmium (Cd^{2+}) into the interstices by forming $Ni_{1-x}Cd_xFe_2O_4$(x = 0.0 and 0.1) as the (Cd^{2+}) has larger ionic radius 0.97Å as compared Ni^{2+} 0.72Å [20]. The incremental lattice parameter can be studied according to the Vegard's law [21].

2. Preparation of $Ni_{1-x}Cd_xFe_2O_4$NPs (x = 0.0 and 0.1)

The wet-chemical approach and the sol gel route were used to create the $Ni_{1-x}Cd_xFe_2O_4$ NPs (x = 0.0 and 0.1). To produce a homogenous sol preparation, the AR-grade nickel nitrate, cadmium nitrate, and ferric nitrate were thoroughly combined in DI water. Citric acid was consumed as a complexant in a 1:3 metal nitrate solution. The blended "sol" was held on a magnetic hotplate and swirled at a moderate speed while at 80 °C. To keep the pH of the solution at 7, ammonia solution (NH_4OH) was gently introduced into the mixture. Eventually, a "sol" transformed into a "gel" and in the beaker, a sticky brown gel was created. The solution was raised to the next intermediate stage and the self-ignition took place as a result of the temperature being slightly raised to 120 °C. The self-ignited constituents are propelled to burnout automatically according to the propellant chemistry, and eventually it gives a fine powder of $Ni_{1-x}Cd_xFe_2O_4$ NPs (x= 0.0 and 0.1) that was crushed, sintered, and used for further characterization. The acquired samples received a total dose of 50 Mrad of gamma radiation in the gamma chamber..

3. Characterization techniques

The thermal analysis for the obtained $Ni_{1-x}Cd_xFe_2O_4$ (x= 0.0 and 0.1) NPs was carried out by TGA-DTA curve; at a temperature region of 0 - 1000 °C (with a heat flow rate 5 °C/min) by Thermal (TGA) Analyzer (TG-DTA-DSC) TA Inc; SDT- 2790.The UV-Vis spectra of γ-irradiated $Ni_{1-x}Cd_xFe_2O_4$ (x= 0.0 and 0.1) NPs were carried out by using a UV-Vis spectrophotometer: Make: JASCO make V-750; Serial No. D084261799 from 1000 Å to 200 Å. In the nanometer scale; photometric mode: absorbance unit; with a measuring range 900 - 190 along X-axis; the first point obtained at 0.01473 max. at 0.20956 and min at -0.34010;Data interval= 0.2 nm; Bandwidth=2.0 nm; Response=0.96 sec; Scan mode: Continuous; Scan speed: 400 nanometer per minute. Raman spectroscopy was carried out by HORIBA LabRAM Soleil™

4. Results and characterization output

4.1. Thermal analysis(TGA)

To determine the processing temperature for the compositional stoichiometry created for the experiment, the TGA of γ-irradiated $Ni_{1-x}Cd_xFe_2O_4$(x=0.0 and 0.1) was performed. Thermo gravimetric is employed to specify temperature dependence, weight loss, and heat flow for a wide range of materials, as well as to provide supplemental data for the most popular thermal technique, DSC. In this method, the sample is typically heated steadily under synthetic air or nitrogen (N_2), and the difference in sample mass is assessed. A drop in sample mass suggests that the material under investigation has deteriorated. The material's reaction with the oxygen in synthetic air, however, might lead to a mass gain. This technique is capable of analyzing samples that exhibit mass gain or loss as a result of breakdown, oxidation, or volatile loss. The thermal analysis of the prepared $Ni_{1-x}Cd_xFe_2O_4$ (x= 0.0 and 0.1) is depicted in **Fig. 1(a).** SDT- 2790 in atmosphere at a temperature region of ~25~1000 C (5 °C / min) aimed to estimate the thermal processing temperatures for the production of $Ni_{1-x}Cd_xFe_2O_4$ (x= 0.0 and 0.1). The decomposition of the precursors takes place up to 800 °C. The $Ni_{1-x}Cd_xFe_2O_4$ (x=0.0 and 0.1) specimen has released H_2O molecules, as seen by the endothermic peak at 275 °C. The multiple processes, including oxidation and the entire production of the final product, were responsible for the exothermic peak that was found between 150 °C and 600 °C. Several different types of literature claim that the precursors underwent thermal breakdown at temperatures around 600 °C. However, it was anticipated that production impurities could occur within this range. **Fig. 1(b)** depicts the Energy dispersive X-ray Analysis of γ- $Ni_{1-x}Cd_xFe_2O_4$ (x= 0.1), and the elemental constituency has been identified.

(a)

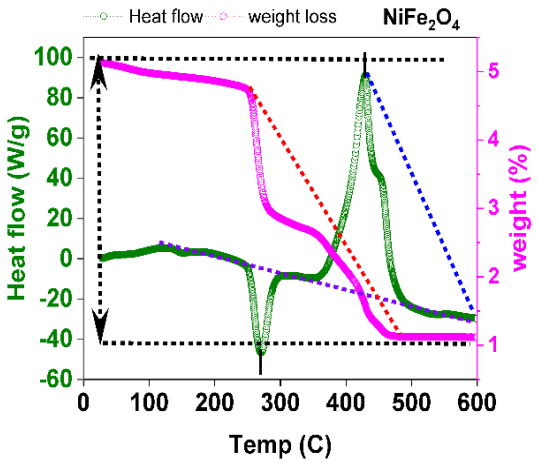

Fig. 1(a). Thermogravimetric analysis (TGA) of γ-irradiated$NiFe_2O_4$

(b)

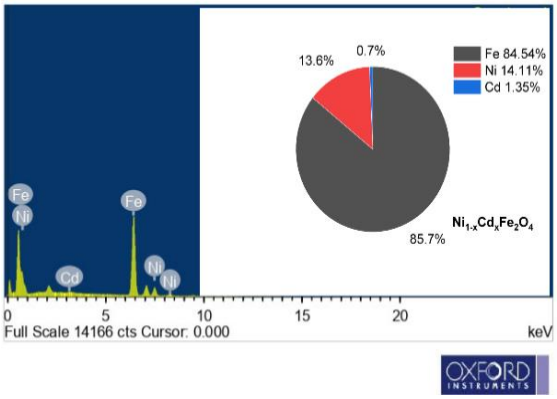

Fig. 1(b). Energy dispersive X-ray Analysis of γ- $Ni_{1-x}Cd_xFe_2O_4$ (x= 0.1)

4.2. Raman spectroscopy γ-irradiated $Ni_{1-x}Cd_xFe_2O_4$ (x= 0.0 and 0.1)

The Raman spectroscopic analysis of -irradiated $Ni_{1-x}Cd_xFe_2O_4$ (x=0.0 and 0.1) was carried out for a number of intense vibrationally active Raman modes, including $3T_{2g1}$, T_{2g2} , T_{2g2},E_g, and A_{1g} modes; of the molecular structure that could be computed to be for the formation of (Fd_{3m-1}) cubic spinel structure[22]. In **Fig. 2 (a) and (b)**, depicts the active Raman modes for the (A)-site associated with the wave number > 600 cm^{-1}; that belongs to F_d. The [B]-site is associated to the wave number that are belongs to the D_{3d} point group [23]. It could be seen that A_{1g} reflection lies at 660 ±10 cm^{-1} indicating the stretching of Fe^{3+}trivalent ion and O^{2-}divalent ions in the (A)-sites [24]. The other reflection consumes lower energy; that raised due to the veering of O^{2-} ions in comparison to that of the Fe ion at (A)-sites; and . the stretching complexants of the Fe-O and Ni-O in $NiFe_2O_4$ NPs are not prominent in this spectra [25].

(a)

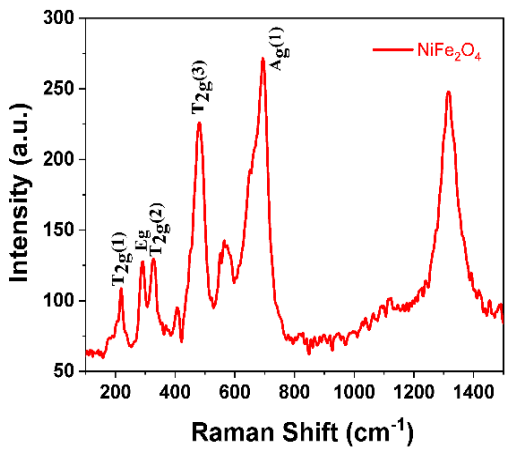

Fig. 2(a). Active Raman mode spectra of γ-irradiated$NiFe_2O_4$

(b)

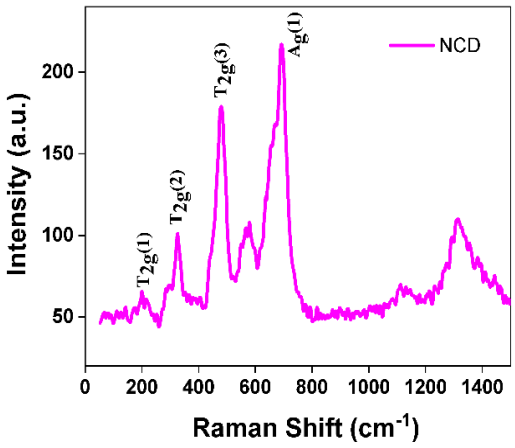

Fig. 2(b). Active Raman mode of γ-$Ni_{1-x}Cd_xFe_2O_4$ (x= 0.1)

4.3. UV-Vis spectra of γ-irradiated $Ni_{1-x}Cd_xFe_2O_4$ (x= 0.0 and 0.1)

TheUltra Violet range-Vis spectra of γ-irradiated $Ni_{1-x}Cd_xFe_2O_4$ (x= 0.0 and 0.1) was taken using a UV-Vis spectrophotometer: JASCO from 900 Å - 190 Å. **Fig. 3 (a) and (b)** depicts the UV absorbance spectra; highlighting a maximum absorbance lay in UV band of electromagnetic spectrum of light. The UV absorbance of $NiFe_2O_4$ ranges at λ = ~292.4 Å; ~340.2 Å high peaked at ~340.2 Å; peak height at 0.06882 has been depicted in **Table 1.**Similarly, for $Ni_{1-x}Cd_xFe_2O_4$ (x= 0.1) ~340.77 Å; ~563.28 Å; ~700 Å high peaked at ~340,77 Å; peak height ~ 0.087.

Table 1. Peak details of the of UV-Vis absorbance spectra γ-irradiated $Ni_{1-x}Cd_xFe_2O_4$ (x= 0.0 and 0.1).

Peak	Area	Area IntgP(%)	Row Index	Beginning X	Ending X	FWHM	Centre	Height
292.4	4.16127	8.54428	3039	289.2	340	50.6	292.4	0.09646
340.2	2.13307	4.3798	2800	340	412.2	28.00599	340.2	0.06882

(a)

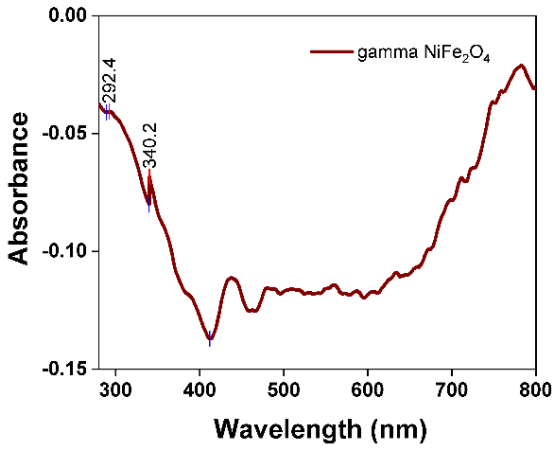

Fig. 3(a). Ultra violet –visible absorbance of γ-irrad $NiFe_2O_4$

(b)

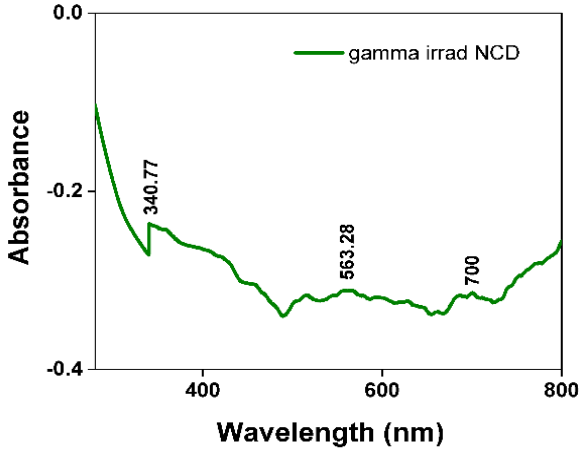

Fig. 3(b). Ultra violet –visible absorbance of γ- $Ni_{1-x}Cd_xFe_2O_4$ (x= 0.1)

4.4. Bandgap of γ-irradiated $Ni_{1-x}Cd_xFe_2O_4$ (x= 0.0 and 0.1)

The Utilizing the Kubelka-Munkfunction F(R), which is denoted by the formula, the direct bandgap energy (Eg) of -irradiated $Ni_{1-x}Cd_xFe_2O_4$ (x= 0.0 and 0.1) was computed: $F(R) = a = (1-R)^2/2R$; [26, 27];. where, α = absorption constant equivalent to the Tauc's equation; R = defused reflectance; The extrapolated plot of $[\alpha h\nu]^2$ is shown in **fig. 4(a) and (b)**; that represents the optical bandgap (Eg) parameters were found to be 1.41 eV for γ-irradiated $NiFe_2O_4$ and 1.5 eV for -irradiated $Ni_{1-x}Cd_xFe_2O_4$; to study the quantum confinement effect within the γ-irradiated $Ni_{1-x}Cd_xFe_2O_4$ (x= 0.0 and 0.1).

(a)

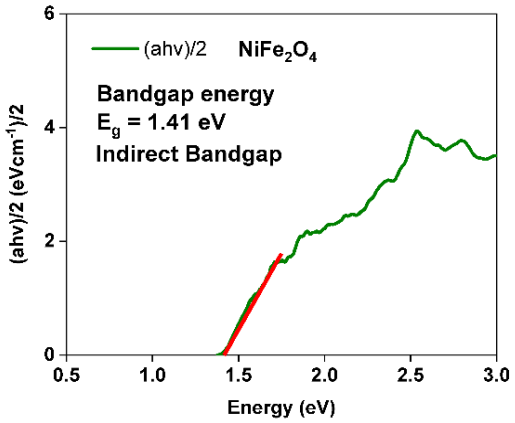

Fig. 4(a). Tauc's extrapolated plot using the Kubelka-Munkfunction F(R) of γ-irrad $NiFe_2O_4$

(b)

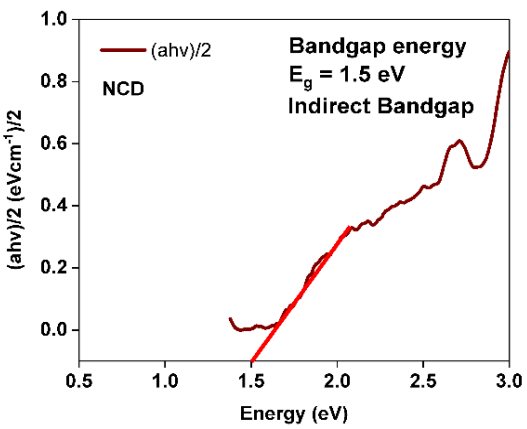

Fig. 4(b). Tauc's extrapolated plot using the Kubelka-Munkfunction F(R) of γ-irrad $Ni_{1-x}Cd_xFe_2O_4$ (x= 0.1)

5. Conclusions

This study used wet chemical synthesis to create $Ni_{1-x}Cd_xFe_2O_4$ NPs for x=0.0 and 1.0, utilising the sol-gel technique and using ($C_6H_5O_7^{3-}$) as a fuel while maintaining pH 7. $Ni_{1-x}Cd_xFe_2O_4$ has an exothermic peak in the TGA that ranges from 275 °C to 600 °C, and an endothermic peak at 150 °C. The existence of the active Raman modes $3T_{2g1}$, T_{2g2}, T_{2g2}, E_g;and A_{1g} reflection in the Raman spectra of the γ-irradiated $Ni_{1-x}Cd_xFe_2O_4$ NPs has supported the ferrite phase's creation. The (A)-site's A_{1g} active Raman mode is located at a distance of 660 ±10 cm^{-1}. Peaks in the UV-Vis spectroscopic absorption of $Ni_{1-x}Cd_xFe_2O_4$NPs exposed to gamma radiation were observed at ~340.77 Å; ~563.28 Å, and the bandgap determined by Touc's plot using the Kubelka-Munkfunction F(R) was reported in the specific range between ~1.41 eV and ~1.5 eV.

Acknowledgments

Dr. Babasaheb Ambedkar Marathwada University, Aurangabad, has provided financing for the project, and the researcher Dr. Manisha Patil is grateful. Likewise, I would like to thank Prof. K.M. Jadhav, who served as the former head of the physics department at the Dr. Babasaheb Ambedkar Marathwada University in Aurangabad, for his invaluable advice.

Reference

[1] D. Salazar, D. Jackson, J.L. Guendon, H. Salinas, D. Morata, V. Figueroa, G. Manríquez, V. Castro, Early evidence (ca. 12,000 BP) for iron oxide mining on the Pacific coast of South America, Current Anthropology, 52 (2011) 463-475.

[2] R. Balasubramaniam, A.R. Kumar, P. Dillmann, Characterization of rust on ancient Indian iron, Current Science, (2003) 1546-1555.

[3] P. Thakur, A. Thakur, Nanomaterials, their Types and Properties, in: Synthesis and Applications of Nanoparticles, Springer, 2022, pp. 19-44.

[4] V. Kirankumar, S. Sumathi, A review on photodegradation of organic pollutants using spinel oxide, Materials Today Chemistry, 18 (2020) 100355.

[5] K.D. Martinson, I.B. Panteleev, A.P. Shevchik, V.I. Popkov, Effect of the Red/Ox ratio on the structure and magnetic behavior of Li0. 5Fe2. 5O4 nanocrystals synthesized by solution combustion approach, Letters on Materials, 9 (2019) 475-479.

[6] N. Rezlescu, E. Rezlescu, P. Popa, E. Popovici, C. Doroftei, M. Ignat, Preparation and characterization of spinel-type MeFe2O4 (Me= Cu, Cd, Ni and Zn) for catalyst applications, Materials Chemistry and Physics, 137 (2013) 922-927.

[7] R. Anu, K. Vinod, Study of magnetic and optical transitions in MFe2O4 (M= Co, Zn, Fe, Mn) with spinel structure, Наносистемы: физика, химия, математика, 12 (2021) 481-491.

[8] N. Kumari, S. Kour, G. Singh, R.K. Sharma, A brief review on synthesis, properties and applications of ferrites, in: AIP Conference Proceedings, AIP Publishing LLC, 2020, pp. 020164.

[9] R. Jabbar, S.H. Sabeeh, A.M. Hameed, Structural, dielectric and magnetic properties of Mn+ 2 doped cobalt ferrite nanoparticles, Journal of Magnetism and Magnetic Materials, 494 (2020) 165726.

[10] T. Dippong, E.A. Levei, O. Cadar, Recent Advances in Synthesis and Applications of MFe2O4 (M= Co, Cu, Mn, Ni, Zn) Nanoparticles, Nanomaterials, 11 (2021) 1560.

[11] N. Grimes, The spinels: versatile materials, Physics in Technology, 6 (1975) 22.

[12] H.A. Adeola, S. Sabiu, T.A. Adekiya, R.T. Aruleba, C.E. Aruwa, B.E. Oyinloye, Prospects of nanodentistry for the diagnosis and treatment of maxillofacial pathologies and cancers, Heliyon, 6 (2020) e04890.

[13] X. Zhao, Z. Meng, Y. Wang, W. Chen, C. Sun, B. Cui, J. Cui, M. Yu, Z. Zeng, S. Guo, Pollen magnetofection for genetic modification with magnetic nanoparticles as gene carriers, Nature plants, 3 (2017) 956-964.

[14] S. Dutz, S. Wojahn, C. Gräfe, A. Weidner, J.H. Clement, Influence of sterilization and preservation procedures on the integrity of serum protein-coated magnetic nanoparticles, Nanomaterials, 7 (2017) 453.

[15] K.R. Reddy, P.A. Reddy, C.V. Reddy, N.P. Shetti, B. Babu, K. Ravindranadh, M.V. Shankar, M.C. Reddy, S. Soni, S. Naveen, Functionalized magnetic nanoparticles/biopolymer hybrids: synthesis methods, properties and biomedical applications, Methods in microbiology, 46 (2019) 227-254.

[16] Y. Tao, H.F. Chan, B. Shi, M. Li, K.W. Leong, Light: a magical tool for controlled drug delivery, Advanced Functional Materials, 30 (2020) 2005029.

[17] M. Bengisu, M. Ferrara, Materials that move: smart materials, intelligent design, Springer, 2018.

[18] C. Murugesan, K. Ugendar, L. Okrasa, J. Shen, G. Chandrasekaran, Zinc substitution effect on the structural, spectroscopic and electrical properties of nanocrystalline MnFe2O4 spinel ferrite, Ceramics International, 47 (2021) 1672-1685.

[19] S. Shaat, H. Dawoud, Influence of variation of structural parameters on magnetic properties of Al-substituted Ni spinel ferrite, Journal of Materials Science: Materials in Electronics, 32 (2021) 11536-11546.

[20] P.A. Rao, V. Raghavendra, B. Suryanarayana, T. Paulos, N. Murali, P.P. Varma, R.G. Prasad, Y. Ramakrishna, K. Chandramouli, Cadmium substitution effect on structural, electrical and magnetic properties of Ni-Zn nano ferrites, Results in Physics, 19 (2020) 103487.

[21] M. Rahimi, M. Eshraghi, P. Kameli, Structural and magnetic characterizations of Cd substituted nickel ferrite nanoparticles, Ceramics international, 40 (2014) 15569-15575.

[22] H. Liu, Z. Yu, B. Fu, M. Ran, C. Wu, X. Jiang, R. Guo, Z. Lan, K. Sun, Anisotropic growth and magnetic properties of nickel–zinc ferrite thin film by spin spray deposition, Ceramics International, 47 (2021) 1318-1324.

[23] M.P. Ghosh, S. Sharma, H.K. Satyapal, K. Tanbir, R.K. Singh, S. Mukherjee, Tuning the microstructural, optical and superexchange interactions with rare earth Eu doping in nickel ferrite nanoparticles, Materials Chemistry and Physics, 241 (2020) 122383.

[24] M. Anupama, N. Srinatha, S. Matteppanavar, B. Angadi, B. Sahoo, B. Rudraswamy, Effect of Zn substitution on the structural and magnetic properties of nanocrystalline NiFe2O4 ferrites, Ceramics International, 44 (2018) 4946-4954.

[25] H. Kardile, S.B. Somvanshi, A.R. Chavan, A. Pandit, K. Jadhav, Effect of Cd2+ doping on structural, morphological, optical, magnetic and wettability properties of nickel ferrite thin films, Optik, 207 (2020) 164462.

[26] S.A. Jadhav, S.B. Somvanshi, M.V. Khedkar, S.R. Patade, K. Jadhav, Magneto-structural and photocatalytic behavior of mixed Ni–Zn nano-spinel ferrites: visible light-enabled active photodegradation of rhodamine B, Journal of Materials Science: Materials in Electronics, 31 (2020) 11352-11365.

[27] T. Vidya Sagar, T. Subba Rao, N. Raghuram, Temperature dependent structural, morphological, FTIR, optical, magnetic properties of NiMgZn ferrites, Наносистемы: физика, химия, математика, 11 (2020) 434-443.